ELSEVIER

Journal of Alloys and Compounds 434–435 (2007) 505–508

Journal of ALLOYS AND COMPOUNDS

www.elsevier.com/locate/jallcom

Cold compaction of metal–ceramic (ferromagnetic–antiferromagnetic) composites using high pressure torsion

E. Menéndez [a], J. Sort [b,*], V. Langlais [a], A. Zhilyaev [c], J.S. Muñoz [a], S. Suriñach [a], J. Nogués [b], M.D. Baró [a]

[a] *Departament de Física, Universitat Autònoma de Barcelona, 08193 Bellaterra, Spain*
[b] *Institució Catalana de Recerca i Estudis Avançats (ICREA) and Departament de Física, Universitat Autònoma de Barcelona, 08193 Bellaterra, Spain*
[c] *Institute for Metals Superplasticity Problems of the Russian Academy of Science, 39 Khalturin St., Ufa 450001, Russia*

Available online 28 September 2006

Abstract

Metal–ceramic powder mixtures consisting of Co (ferromagnetic) and NiO (antiferromagnetic), at the 1:1 weight ratio, have been compacted by high pressure torsion (HPT) both with and without a prior ball milling (BM) process. The compaction causes a strong reduction of the crystallite sizes, introduces large amounts of stacking faults in the metal and induces a phase transformation from the fcc to the hcp Co allotropes. An enhancement of the coercivity is observed, which is ascribed to the Co particle size refinement, the increase of stacking faults and the magnetic coupling between Co and NiO. Furthermore, ball milled Co–NiO powders compacted by HPT exhibit values of the Vickers microhardness almost twice the value obtained for pure Co subjected to HPT.

Keywords: Nanostructured materials; Mechanical alloying; Magnetization; X-ray diffraction

In recent years, high pressure torsion (HPT) has established itself as a processing route for the cold-consolidation of different types of pure metals and alloys [1–3]. Contrary to other methods, such as hot-isostatic pressing, HPT allows obtaining almost fully dense disks while circumventing particle growth. This yields disk-shaped bulk materials with outstanding properties owing to their preserved nanocrystalline character, such as large microhardness [4] or high strain-rate superplasticity [5]. HPT also allows compacting amorphous powders [6]. So far, this technique has been rarely used to consolidate metal–ceramic powder mixtures (cermets) [7–9]. Typically, cermet composites have applications as cutting tools or coating layers with large corrosion and wear resistance [10]. In all the few cermets consolidated by HPT the weight fraction of the ceramic counterpart does not exceed 15 vol.% and it is added to the metal mainly to inhibit its grain growth during posterior annealing.

From the magnetic point of view, the coupling between ferromagnetic (FM) and antiferromagnetic (AFM) materials, typically results in a shift of the hysteresis loop [11–13] and a coercivity enhancement. This phenomenon has widespread applications, such as to enhance hard magnetic properties [14] or to develop spin-valves or magnetic tunnel junctions structures [11,15].

In this article, we use HPT to compact metal–ceramic powder mixtures (Co–NiO) with a large percentage of ceramic (i.e. 50 wt.%). Although the compaction is achieved both with and without a prior ball milling (BM) process, a good intermixing between the Co and NiO is only accomplished by subjecting the powders to BM prior to HPT.

1. Experimental details

Metal (Co, 99.5%, <44 μm)–ceramic (NiO, 99%, <100 μm) powder mixtures, in a weight ratio of 1:1, were compacted by HPT to obtain disks of approximately 1 cm diameter and 300 μm thickness. Two types of samples were prepared: (i) as-received Co and NiO powders were simply mixed and subsequently compacted by HPT and (ii) Co–NiO where the powders were first ball-milled for 25 h and then compacted by HPT. The BM was performed in a planetary ball mill, under Ar atmosphere, using stainless steel vials and balls and a ball-to-powder ratio of 2:1. The HPT process was carried out in a modified *Bridgeman* cylindrical anvil type device, subjecting the powder mixtures to a five whole-turn torsion under an applied pressure of 6 GPa at room temperature, i.e. without purposely heating the anvils during the compaction. For comparison, pure Co powders were also subjected to HPT. For the HPT procedure, an unconstrained device was used, which allows the specimen to flow outwards under the

* Corresponding author. Tel.: +34 93 581 14 01; fax: +34 93 581 21 55.
E-mail address: jordi.sort@uab.es (J. Sort).

0925-8388/$ – see front matter © 2006 Elsevier B.V. All rights reserved.
doi:10.1016/j.jallcom.2006.08.142

applied pressure so that no back-pressure is introduced into the system during the compaction [3].

The morphology of the composites was examined using a scanning electron microscope (SEM). The microstructural parameters were evaluated by adjusting X-ray diffraction (XRD) patterns (recorded using Cu Kα radiation) with a full pattern fitting procedure [16,17]. Hysteresis loops were acquired by means of a vibrating sample magnetometer. The disks were subject to a field cooling (FC) process, under an applied magnetic field of 0.5 T, from temperatures ranging from 300 to 730 K. Finally, the Vickers microhardness, H_V, was determined using a load of 0.05 Kg.

2. Results and discussion

Fig. 1 shows the SEM images of Co–NiO disks, obtained by subjecting the initial powders (without BM) to HPT (in (a)) and after compacting by HPT the previously ball-milled powder mixture (in (d)). Fig. 1(b and e) are the Co energy-dispersive X-ray (EDX) mappings, while Fig. 1(c and f) are the Ni EDX mappings, corresponding to Fig. 1(a and d), respectively. In the two types of disks, Co particles tend to become elongated following the shear flows of the material during the HPT compaction. However, due to the plasticity of Co, it is more difficult to refine its particle size than for NiO. Only when Co and NiO are ball-milled together before the HPT, isolated Co particles become embedded in the NiO matrix. This microstructure yields large amounts of interfaces between the FM and AFM phases. Interestingly, in both cases, no pronounced differences are found between the morphology of the disk center and edge.

From Fig. 2, it can be seen that the starting Co is a mixture of hcp and fcc phases. During HPT, the fcc phase transforms into hcp. This mechanically driven phase transformation, which has also been reported in BM and/or HPT of pure Co [4], is accompanied by a strong reduction in the crystallite size and an increase of the microstrains. Furthermore, as can be seen in Fig. 2, not all Co diffraction peaks exhibit the same broadening. This is indicative of the existence of stacking faults. According to Warren's description of stacking faults, two types of these planar defects can be distinguished in a hcp structure, deformation and twin faults, whose probabilities are denoted as α and β, respectively (where $1/\alpha$ and $1/\beta$ designate the number of layers between two consecutive faults) [18]. Listed in Table 1 are the crystallite sizes, microstrains and stacking fault probabilities for the different samples. When Co is mixed with NiO before being subjected to HPT, the obtained crystallite size is much smaller than that of compacted pure Co powders, suggesting that NiO favors the fracturing of the metallic particles during HPT. In addition, HPT tends to increase the amount of deformation faults at the expense of twin faults. This can be ascribed to the fact that the stress required to generate twinning increases more rapidly than the yield stress for slip when crystallite size is reduced, as

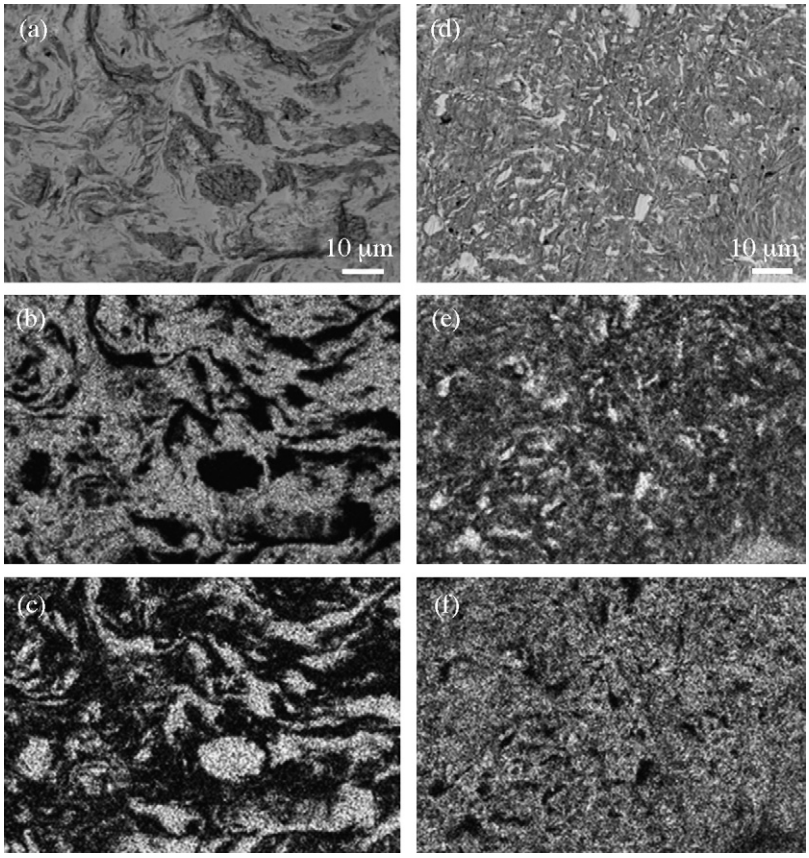

Fig. 1. (a) SEM image obtained using backscattered electrons from the unmilled Co–NiO powders compacted by HPT. Shown in (b and c) are the corresponding Co and Ni EDX mappings. (d) SEM image of the Co–NiO disks obtained by ball milling and subsequent HPT. The images in (e and f) are the corresponding Co and Ni EDX mappings.

Table 1
Summary of the relevant structural parameters (crystallite sizes, $\langle d \rangle$; microstrains, $\langle \varepsilon^2 \rangle^{1/2}$; deformation, α and twin, β, stacking fault probabilities) of the diverse phases for the different types of samples, including the initial Co powders

	Initial Co powder	Co HPT	Co–NiO HPT	Co–NiO BM + HPT
$\langle d \rangle_{\text{hcp-Co}}$ (±5 nm)	97	54	32	20
$\langle d \rangle_{\text{fcc-Co}}$ (±5 nm)	114	–	–	–
$\langle d \rangle_{\text{NiO}}$ (±5 nm)	–	–	48	9
$\langle \varepsilon^2 \rangle^{1/2}_{\text{hcp-Co}}$ ($\pm 2 \times 10^{-4}$)	–	23×10^{-4}	15×10^{-4}	47×10^{-4}
$\alpha_{\text{hcp-Co}}$ ($\pm 1 \times 10^{-3}$)	2×10^{-3}	6×10^{-3}	8×10^{-3}	–
$\beta_{\text{hcp-Co}}$ ($\pm 1 \times 10^{-3}$)	15×10^{-3}	11×10^{-3}	7×10^{-3}	–

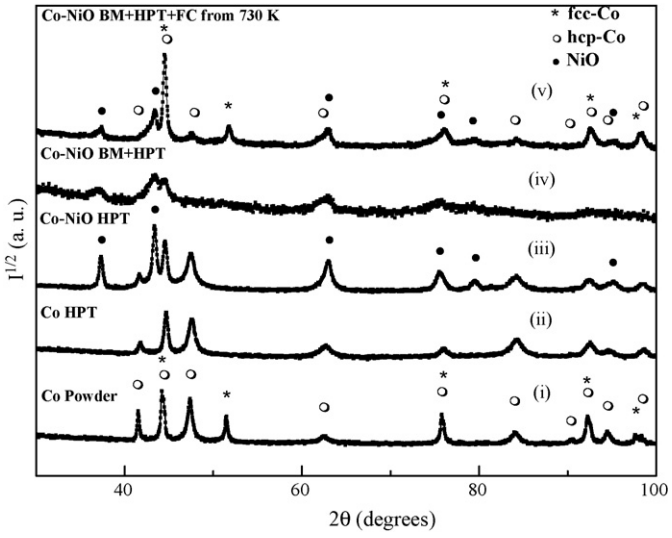

Fig. 2. XRD patterns of: (i) the initial Co powders, (ii) Co powders subjected to HPT, (iii) Co–NiO compacted by HPT, (iv) Co–NiO BM and subsequently compacted by HPT and (v) Co–NiO BM, compacted by HPT, annealed for 0.5 h at 730 K and field-cooled (FC) to room temperature. Indicated in figure are the main XRD peaks corresponding to hcp-Co, fcc-Co and NiO phases.

it occurs during HPT [4]. In the Co–NiO BM + HPT sample, the diffraction peaks become very broad (see Fig. 2), hence making the determination of stacking fault probabilities unreliable. The combination of the two processing routes induces an obvious reduction in the crystallite size, together with an increase of the microstrains, as compared to HPT alone. Fig. 2 also shows that when Co–NiO disks are heated to high temperatures (e.g. 730 K), fcc-Co reappears. Annealing at intermediate temperatures (e.g. 475 K) already causes structural relaxation of the HPT disks, which manifests, as shown in Table 2, by a slight increase in the crystallite sizes and a decrease in the microstrains. The amount of fcc-Co in Co–NiO BM + HPT is larger than for the HPT one, probably because of the rather small particle sizes achieved in this sample.

These structural features determine the magnetic behavior of Co and Co–NiO powders subjected to HPT. Namely, when Co powders (without NiO) are compacted by HPT, their coercivity increases considerably, from 16.0 mT in the as-received material to 23.6 mT in the HPT disks. This is mainly due to the allotropic phase transformation from fcc to hcp-Co that occurs during HPT, since the hcp phase exhibits a larger magnetocrystalline anisotropy, although the presence of stacking faults also contributes to the H_C enhancement [19]. An even larger coercivity value, i.e. $\mu_0 H_C = 27.3$ mT, is obtained when Co is compacted together with NiO. This is probably related to the smaller Co crystallite size achieved and the presence of NiO grains, all of which can act as barriers for domain wall propagation during magnetization reversal. A significant H_C enhancement (up to $\mu_0 H_C = 33.0$ mT) is achieved if Co–NiO are ball-milled prior to the HPT compaction. In this case, the Co particles become embedded in the NiO matrix and, consequently, the exchange interactions between Co grains, which typically have a detrimental effect in H_C, are reduced. Moreover, Co particles tend to acquire elongated shapes, which can also contribute to H_C by means of an increase of the magnetic shape anisotropy. The coupling between Co and NiO could also favor the H_C enhancement. However, to induce such a coupling usually a field cooling process from above the blocking temperature, T_B, of the AFM grains is required. Typically, a distribution of T_B, up to the Néel temperature (550 K for NiO), exists in granular AFM [11–13,20].

Plotted in Fig. 3 is the dependence of H_C on the field cooling temperature, T_{FC}, for unmilled and BM Co–NiO powders, both compacted by HPT. As can be seen in figure, although H_C progressively decreases with T_{FC} in the unmilled Co–NiO, a peak in H_C around 600–650 K is observed for the BM + HPT disk. The decrease of H_C with T_{FC} can be ascribed to the structural relaxation that occurs in Co upon heating. The reduction of H_C for $T_{FC} < 450$ K is exacerbated for the BM + HPT sample, where

Table 2
Summary of the relevant structural parameters obtained for the HPT and BM + HPT Co–NiO disks, before and after field cooling (FC) from $T_{FC} = 475$ and 730 K to room temperature

	No FC	FC from $T = 475$ K	FC from $T = 730$ K
Co–NiO HPT			
fcc (wt.%)	0	0	20
$\langle d \rangle_{\text{hcp-Co}}$ (nm) (±5 nm)	32	43	55
$\langle d \rangle_{\text{NiO}}$ (nm) (±5 nm)	48	56	63
$\langle \varepsilon^2 \rangle^{1/2}_{\text{hcp-Co}}$ ($\pm 2 \times 10^{-4}$)	15×10^{-4}	14×10^{-4}	4×10^{-4}
Co–NiO BM + HPT			
fcc (wt.%)	0	7	39
$\langle d \rangle_{\text{hcp-Co}}$ (nm) (±5 nm)	20	52	77
$\langle d \rangle_{\text{NiO}}$ (nm) (±5 nm)	9	17	14
$\langle \varepsilon^2 \rangle^{1/2}_{\text{hcp-Co}}$ ($\pm 2 \times 10^{-4}$)	47×10^{-4}	35×10^{-4}	3×10^{-4}

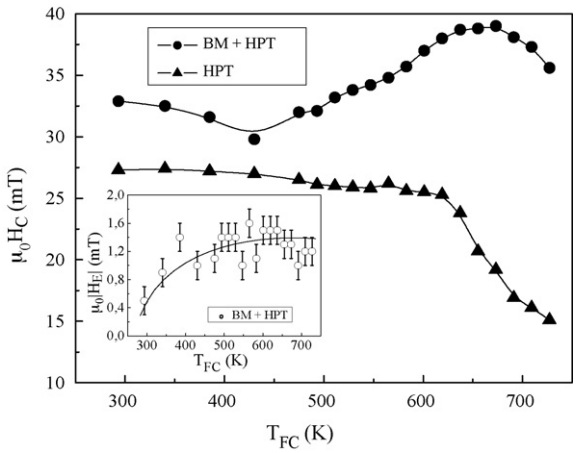

Fig. 3. Dependence of H_C on the field cooling temperature, T_{FC}, for unmilled and ball-milled Co–NiO powders, both compacted by HPT. The inset shows the dependence of the exchange bias field, H_E, on T_{FC} for the BM + HPT Co–NiO sample. The lines are guides to the eye.

larger amount of structural defects have been accumulated. In both disks, for $T_{FC} > 650$ K the decrease of H_C becomes more pronounced since hcp-Co starts to transform into fcc-Co. Contrary to the unmilled Co–NiO, an increase in H_C is observed for the ball-milled Co–NiO powders compacted by HPT in the T_{FC} interval ranging from 450 to 650 K. This H_C enhancement is probably due to FM–AFM coupling. The existence of such a coupling is confirmed by the presence of hysteresis loop shifts (see inset of Fig. 3), which are not observed in the HPT disk obtained from unmilled Co–NiO.

Microhardness tests were carried out for pure Co and BM Co–NiO powders consolidated by HPT. An enhancement of H_V was observed in the cermet composite, where H_V values as high as 9 GPa were achieved, much larger than for pure Co (where $H_V = 5$ GPa) and close to H_V of some Co/WC cermet nanocomposites [21]. The large H_V in the BM + HPT Co–NiO can be ascribed not only to the presence of the ceramic counterpart but also to the Co crystallite size refinement and the large amounts of stacking faults accumulated (i.e. the Hall–Petch relationship) [4].

3. Conclusions

In summary, the structural, magnetic and mechanical properties of Co–NiO powder mixtures consolidated by HPT have been investigated. Our work demonstrates the efficiency of severe plastic deformation routes to consolidate metal–ceramic mixtures while preventing crystal growth, thus allowing the resultant bulk disks to exhibit some enhanced properties due to their nanocrystalline nature.

Acknowledgements

The authors wish to thank L. Lutterotti for providing the MAUD program for Rietveld refinement of the XRD data. Partial financial support from the INTAS 03-51-3779, the RFBR 05-03-32233-a, the HPRN-CT 2002-00296, the 2005-SGR-00401 and the MAT-2004-01679 research projects is acknowledged. E.M. acknowledges his FPI fellowship (BES-2005-8696) from the Spanish Ministry of Science and Education, co-financed by the E.S.F.

References

[1] R.Z. Valiev, R.S. Mishral, J. Grozal, A.K. Mukherjee, Scripta Mater. 34 (1996) 1443–1448.
[2] R.Z. Valiev, R.K. Islamgaliev, I.V. Alexandrov, Prog. Mater. Sci. 45 (2000) 103–189.
[3] B. Baretzky, M.D. Baró, G.P. Grabovetskaya, J. Gubicza, M.B. Ivanov, Y.R. Kolobov, T.G. Langdon, J. Lendvai, A.G. Lipnitskii, A.A. Mazilkin, A.A. Nazarov, J. Nogués, I.A. Ovidko, S.G. Protasova, G.I. Raab, A. Revesz, N.V. Skiba, J. Sort, M.J. Starink, B.B. Straumal, S. Suriñach, T. Ungar, A.P. Zhilyaev, Rev. Adv. Mater. Sci. 9 (2005) 45–108.
[4] J. Sort, A. Zhilyaev, M. Zielinska, J. Nogués, S. Suriñach, J. Thibault, M.D. Baró, Acta Mater. 51 (2003) 6385–6393.
[5] X. McFadden, R.S. Mishra, R.Z. Valiev, A.P. Zhilyaev, A.K. Mukherjee, Nature 398 (1999) 684–686.
[6] J. Sort, D.C. Ile, A.P. Zhilyaev, A. Concustell, T. Czeppe, M. Stoica, S. Suriñach, J. Eckert, M.D. Baró, Scripta Mater. 50 (2004) 1221–1225.
[7] I.V. Alexandrov, Y.T. Zhu, T.C. Lowe, R.K. Islamgaliev, R.Z. Valiev, Nanostruct. Mater. 10 (1998) 45–54.
[8] R.K. Islamgaliev, W. Buchgraber, Y.R. Kolobov, N.M. Amirkhanov, A.V. Sergueeva, K.V. Ivanov, G.P. Grabovetskaya, Mater. Sci. Eng. A 319–321 (2001) 872–876.
[9] R. Kuzel, Z. Matej, V. Cherkaska, J. Pesicka, J. Cízek, I. Procházka, R.K. Islamgaliev, J. Alloys Compd. 378 (2004) 242–247.
[10] S. Suresh, A. Mortensen, Int. Mater. Rev. 42 (1997) 85–116.
[11] J. Nogués, I.K. Schuller, J. Magn. Magn. Mater. 192 (1999) 203–232.
[12] J. Nogués, J. Sort, V. Langlais, S. Doppiu, B. Dieny, J.S. Muñoz, S. Suriñach, M.D. Baró, S. Stoyanov, Y. Zhang, Int. J. Nanotechnol. 2 (2005) 23–42.
[13] J. Nogués, J. Sort, V. Langlais, S. Skumryev, S. Suriñach, J.S. Muñoz, M.D. Baró, Phys. Rep. 422 (2005) 65–117.
[14] J. Sort, J. Nogués, X. Amils, S. Suriñach, J.S. Muñoz, M.D. Baró, Appl. Phys. Lett. 75 (1999) 3177–3179.
[15] B. Dieny, V.S. Speriosu, S.S.P. Parkin, B.A. Gurney, D.R. Wilhoit, D. Mauri, Phys. Rev. B 43 (1991) 1297–1300.
[16] R.A. Young, The Rietveld Method, International Union of Crystallography, University Press, Oxford, 1995.
[17] L. Lutterotti, S. Gialanella, Acta Mater. 46 (1997) 101–110.
[18] B.E. Warren, X-ray Diffraction, Addison-Wesley, Reading, Massachusetts, 1969.
[19] J. Sort, S. Suriñach, J.S. Muñoz, M.D. Baró, M. Wojcik, E. Jedryka, S. Nadolski, N. Sheludko, J. Nogués, Phys. Rev. B 68 (2003) 014421.
[20] S. Soeya, T. Imagawa, K. Mitsuoka, S. Narishige, J. Appl. Phys. 76 (1994) 5356–5360.
[21] R.S. Lima, J. Karthikeyan, C.M. Kay, J. Lindemann, C.C. Berndt, Thin Solid Films 416 (2002) 129–135.